

Autonomous readout ASIC with 169dB input dynamic range for amperometric measurement

Wei Onn Ting, Sara S. Ghoreishizadeh

Department of Electrical and Electronic Engineering, Imperial College London, SW7 2AZ, UK

Email: andytingweionn@gmail.com, sghoreishizadeh@gmail.com

Abstract—A readout circuit for the measurement of amperometric sensors is presented. The circuit consists of analog frontend (AFE) and an automatic gain adjustment circuit to tune the gain of the AFE according to the input current covering a wide dynamic range of 169dB and a minimum input referred noise of 44 fA. The circuit is implemented in 0.35 μm technology, consumes 5.83 mW from 3.3 V supply voltage and occupies 0.31 mm^2 silicon area.

Index Terms—Amperometric sensing, readout circuit, CMOS, wide dynamic range, automatic gain control

I. INTRODUCTION

A new generation of *Implantable and Wearable Medical devices* (IWeMed) are emerging to enable continuous monitoring of small bio-molecules (e.g. glucose, hormones) in the human body. Such IWeMed technology eliminates the need for blood sampling and, through continuous measurement, addresses unmet clinical needs in predictive diagnostics and self-monitoring and management of health.

An IWeMed has to be small, fully-integrated, and wireless to be minimally invasive. Moreover, it should be able to detect specific group of key metabolites and drugs within a single platform, to accurately monitor the health condition of the patient. Most existing biosensing systems consist of the combination of fluidic systems, sensors and electronic circuits to readout the sensors.

To date, several medical devices use electrochemical sensors. A notable example is the continuous glucose measurement devices for diabetes. The electrochemical sensor work based on the principle of electrochemical detection using probe molecules and enzymes to detect the target analyte. The sensor outputs a current to be measured by the instrumentation electronics. In a multi-analyte sensing device, the sensor currents may vary within a wide range (several decades) [1] and even vary from day to day. Therefore, the instrumentation needs to be tuned for each measurement and each sensor.

Autonomy is a key requirement in developing IWeMed for minimally invasive, low-cost and long-term monitoring of different bio-molecules. However, existing devices are not autonomous because, for instance, the readout electronics requires external tuning to be adjusted to different sensors with different signal levels [2]–[4], and the sensors need frequent re-calibrations to detect their time-varying sensitivity [5]. These require human intervention, imposes extra costs, and ultimately limits the progress of IWeMed technology.

In this work we present the design of a readout circuit capable of automatic self-adjustment to measure currents within a wide dynamic range. An *automatic gain adjustment* (AGA) algorithm is developed and implemented on-chip to eliminate the need for manual tuning. The AGA has been implemented in analog domain before [6]. What we propose here is instead a mixed-signal design that presents the benefit of accurate gain control as well as recording/outputting it together with the data for subsequent data interpretation. The design of the system comprising analog and digital parts is presented in the next section, followed by simulation results in Section III.

II. SYSTEM DESIGN

The readout circuit comprises (i) an *analog frontend* (AFE) capable of measuring currents within a wide dynamic range from 1 pA to 10 μA to cover a wide range of amperometric sensors. The wide range is achieved through several gain settings by changing tunable parameters such as integrating capacitor and the integration time; (ii) A gain adjustment block to determine the correct gain and change the related parameters (capacitance, integration time) in AFE based on the input current; (iii) a 10-bit ADC (from standard AMS library cell) which is activated only after the correct gain setting is determined and set by AGA.

The readout circuit switches between two operation modes: readout mode, where ADC is up and running, and *Automatic gain adjustment* (AGA) mode where the gain is being determined. The AGA circuit also outputs the gain settings that can be used together with the digital output of the ADC to interpret the data.

A. Analogue frontend

A switched-capacitor integrator (SCI) is designed to apply a fixed voltage to the sensor and to measure the sensor current. The SCI architecture is chosen because its parameters can be easily adjusted digitally and its potentially low input-referred noise [7]. The schematic view of the SCI circuit is shown in Fig. 1. It consists of a amplifier, integrating capacitors and switches. A single-stage folded cascode topology is chosen as it provides high gain and ensures stability for a wide range of capacitive load. As shown in Fig. 2, large transistors are used for the input differential pair to achieve high transconductance and minimize flicker noise and mismatch. The dimensions of the transistors are chosen carefully to ensure they operate in the saturation region for a wide range of input currents. The

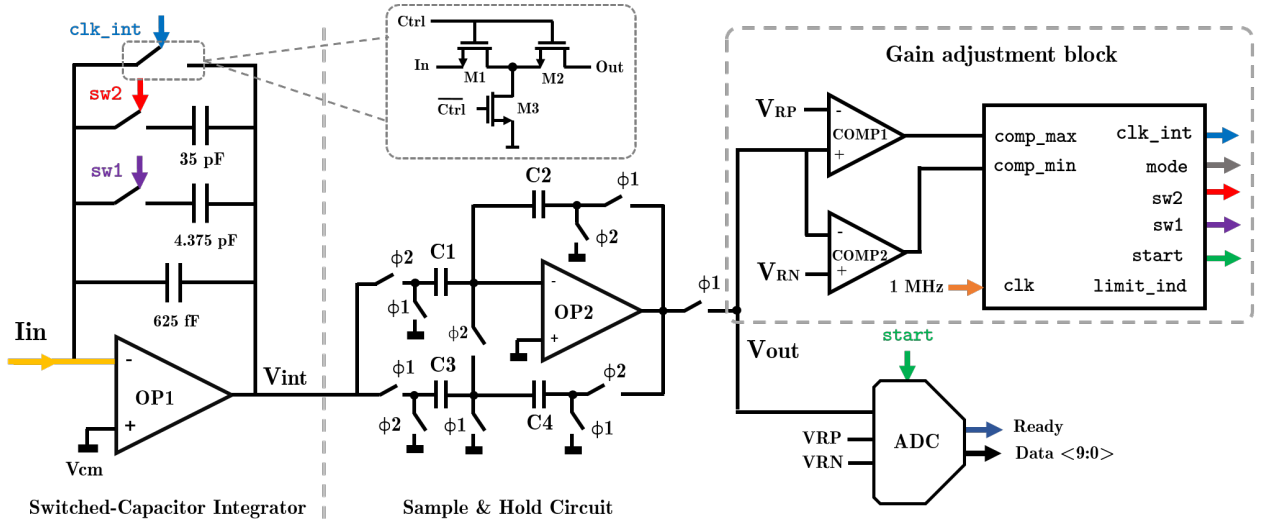


Fig. 1: The block diagram of the proposed readout circuit with automatic gain adjustment

maximum output current of the transconductance amplifier is set close to the maximum input current expected from the sensor ($10 \mu\text{A}$). The simulated gain, -3dB bandwidth and the integrated input referred noise of the amplifier are 92 dB, 7.5 kHz, and $10.4 \mu\text{V}$, respectively.

A low-leakage switch in parallel to the capacitor controls the reset and integration times. When the switch is open, the sensor current flows through the capacitor and generates an output voltage, V_{int} . When the switch is closed, the sensor current flows through the switch and thus the current ensuring there is always a path for the sensor current during both reset and integration phases. The output of the integrator at the end of the integration phase can be calculated by

$$V_{int} = \frac{T_{int} \times I_{in}}{C_{int}} \quad (1)$$

where T_{int} is the integration time, C_{int} is the total feedback capacitance in the TIA, and I_{in} is the input current to the circuit.

To minimize gain error due to the leakage of the switch, a low-leakage switch structure is implemented. This is based on the floating-body techniques where an extra lateral transistor, M3, reduces the leakage maintains a zero voltage across the M1 and M2 during the integration time.

The output of the switched-capacitor integrator is sampled during the integration phase and held during the reset phase, to be sent either to the ADC or to the AGA circuit. The sample and hold circuit is adopted from [8] with correlated double sampling (CDS) to reduce low-frequency (in band) noise. It also has relaxed slew rate demand on the amplifier. Here Φ_1 and Φ_2 are non-overlapping clock phases to drive the switches and correspond to the reset and integration phases, respectively.

B. Automatic Gain Adjustment (AGA)

The whole input current range is divided into eight sub-ranges we refer to as modes. The gain in each mode is

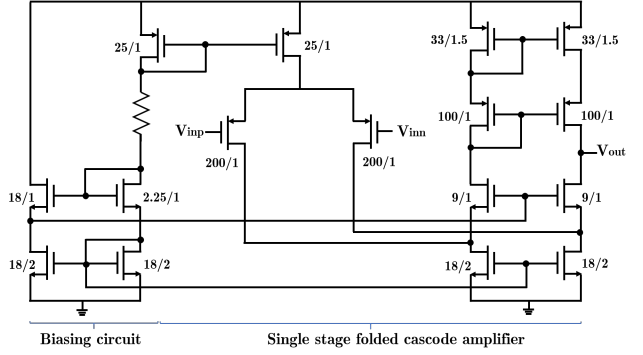


Fig. 2: The schematic of the folded-cascode amplifier used in OP_1 and OP_2

set through adjusting the SCI feedback capacitors and/or the integration time. The gain is chosen so that V_{OUT} remains within a certain range (V_{RN} (1.525 V), V_{RP} (2.65 V)) in order to avoid non-linearity and ensure 10-bit resolution can be achieved in each sub-range using a 10-bit ADC.

The clock waveform is generated in the AGA system based on an external clock of 1 MHz. The generated clock waveforms provide a fixed reset time ($12 \mu\text{s}$) with various integration times ($5 \mu\text{s}$, $40 \mu\text{s}$, $320 \mu\text{s}$, 2.56 ms , 20.48 ms , 164 ms). The AGA circuit also provides the control signals to change the total capacitance to one of 625 fF , 5 pF , 40 pF .

Two comparators compare output of the sample and hold at every clock cycle with an upper (V_{RP}) and a lower threshold (V_{RN}). Here clock-based comparators are chosen to reduce the total power consumption since the comparator is only needed after integration phase. The schematic of the comparator is shown in Fig. 4. The output of the comparators are used to detect in range or out of range samples. The comparison is repeated during N clock cycles to minimize the effect of instantaneous noise on the results. The AGA decides whether there is a need to change the mode only if the percentage of the out of range samples is higher than a threshold value, for

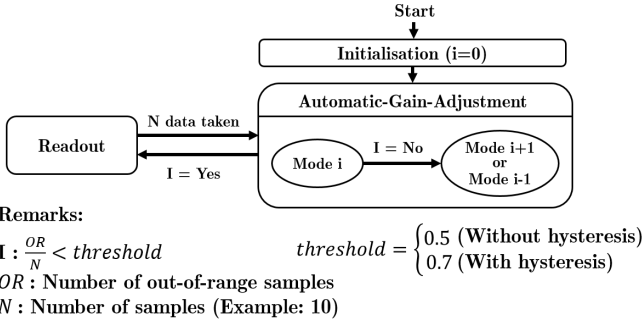


Fig. 3: The state diagram for autonomous gain control.

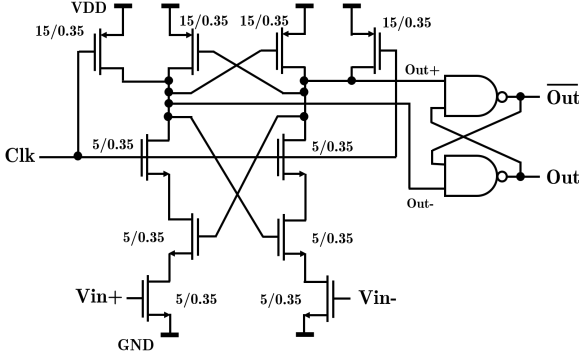


Fig. 4: The schematic of the clocked comparator.

example 50%.

A state diagram for the autonomous gain control algorithm is presented in Fig. 3. At the start-up the circuit enters the AGA mode to determine the mode. Here the initial mode is set to the lowest gain to prevent AFE saturation in case the current belongs to the highest sub-range. Once the mode is determined the *Start* signal is inserted to activate the ADC and the circuit enters the readout mode. The circuit remains in the readout mode for another *N* clock cycles before going back to AGA mode to check/adjust the gain again.

1) *Hysteresis Operation*: To ensure the mode changing during AGA phase does not create mode oscillations, a hysteresis operation is designed and embedded into AGA. The mode oscillation can happen for instance if the input current is in between two modes or if a large electrochemical noise [9] causes multiple crossings between two modes. The hysteresis operation is implemented by altering the out-of-range sample threshold from 50% to 70% every time the AGA phase is activated after a readout phase. The circuit will therefore tend to stay in the current mode unless the change in input current is large and long enough.

III. SIMULATION RESULTS

The circuit is designed in AMS 350nm technology with two poly and four metal layers. The layout is presented in Fig. 5 occupying a total area of 0.31 mm^2 . The whole circuit consumes 5.83 mW from a 3.3 V supply voltage in the initial mode (highest clock frequency, largest capacitor). The minimum input referred noise of the AFE is 44 fA at highest gain. The maximum input current that can be measured with

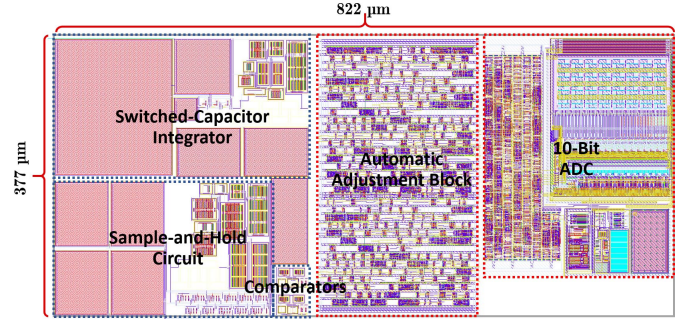


Fig. 5: Complete system layout with annotated floorplan

less than 3% non-linearity is $13 \mu\text{A}$ leading to an overall input dynamic range of 169 dB.

To characterize the system a number of simulations are performed and presented here. Fig. 6 illustrates how the system responds to an input step from 250 nA to 45 nA and reverse (i.e. from mode 1 to mode 2 and reverse). The AGA circuit initially starts from mode 0 and goes to mode 1 to accommodate for 250 nA. After the step change in the current, the mode changes to 2 and gain increases. Then, the circuit enters the readout mode and, after acquiring ten samples, goes back to the AGA mode. Here since the input current has changed significantly the mode changes again.

Parametric simulations is shown in Fig. 7 demonstrating the mode is detected correctly at the end of the first execution of the AGA phase after start-up. The transient simulation shown in Fig. 8 illustrates how the systems changes the mode dynamically during a triangular input current. The delay, $t_{d,ij}$, between when the current crosses between two modes *i* and *j* to the time when the AGA circuit updates the mode is:

$$t_{d,ij} = (N - p)T_{clk,i} + N \times (T_{clk,i+1} + \dots + T_{clk,j}) \quad (2)$$

where $T_{clk,m}$ is the period of the clock in mode *m*, *N* is the number of samples taken in a single AGA cycle (10 in our design), and *p* is the number (between 1 and *N*) of the readout cycle where the current has entered the new sub-range. Although this delay limits the effective bandwidth of the measurement, this is not a concern in IWeMed application due to the slow variations of bio-molecules in/on human body.

A comparison with state-of-the art indicates that out proposed circuit is the first readout circuit that automatically adjusts itself to the input current range (See Table I). The circuit can measure a variety of amperometric sensors without need for tuning to different signal levels.

IV. CONCLUSION

The readout circuit introduced in this report can measure currents within $13 \mu\text{A}$ with a minimum input-referred noise of 44 fA. A mixed-signal gain control system adjusts the gain according to the input current levels. Eight different gain values are achieved by changing the integration time and the integrating capacitance values covering a wide input dynamic range of 169 dB. An embedded hysteresis function is designed to ensure stability when input current is in between two modes as well as in presence of large electrochemical noise.

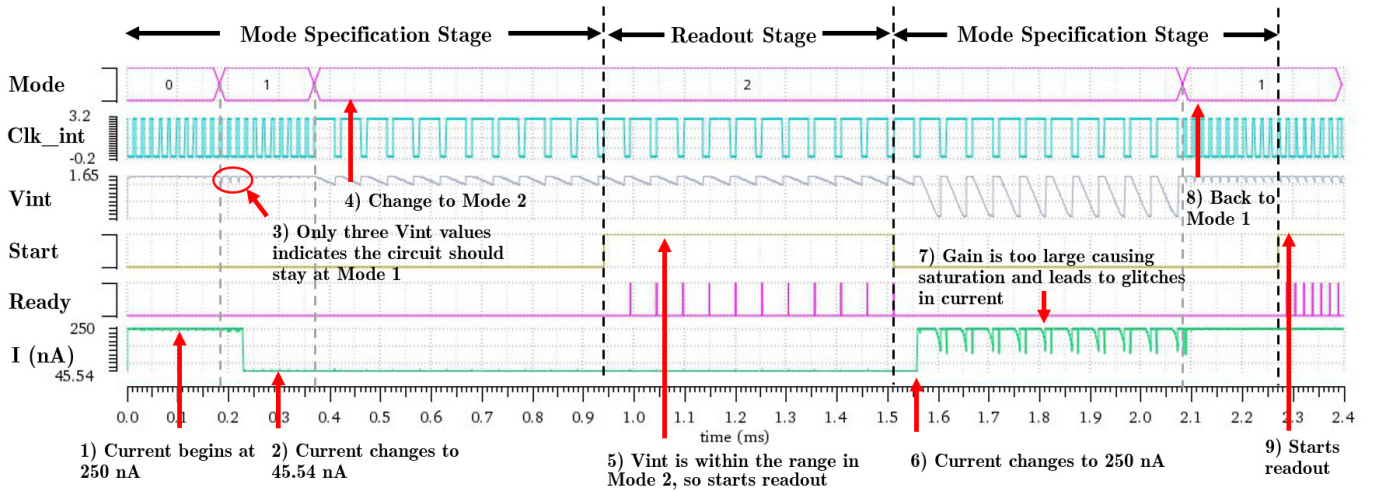


Fig. 6: Readout circuit operation for a step change in the input current. The circuit transitions to a suitable mode based on the input current and performs ADC conversion during readout stage. (Follow steps 1 to 9)

TABLE I. Comparison with the State-of-the-Art

Paper	Technology (μm)	Supply voltage (V)	Input ref. noise (pA)	Max current (μA)	Dynamic range (dB)	Power (mW)	Gain settings	Autonomous adjustments?
TBCAS'13 [2]	0.35	3.3	24	0.35	83	0.19	2	No
TBCAS'07 [3]	0.5	3	0.1	0.5	134	1.27	9	No
TBCAS'16 [4]	0.5	5	0.1	16	164	0.241	4	No
TBCAS'17 [10]	0.35	3.3	0.47	20	153	9.3	4	No
TBCAS'18 [11]	0.5	3.3	7.2	0.11	84	0.021	2	No
This work (simulated)	0.35	3.3	0.044	13	169	5.83	8	Yes

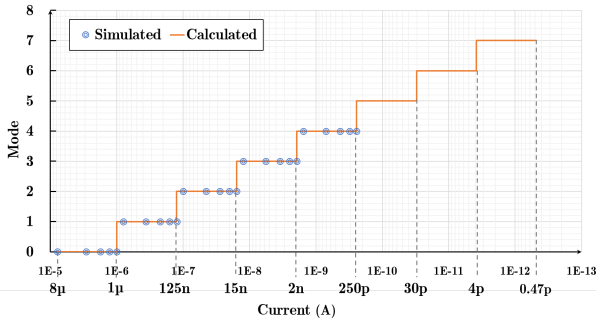


Fig. 7: Simulated characteristics of the whole system showing the final mode determined by AGA circuit vs the input current

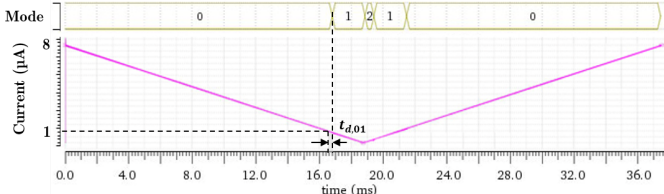


Fig. 8: Mode changes with respect to input current

V. ACKNOWLEDGEMENT

The authors would like to thank Dr Song Luan and Miguel Cacho Soblechhero for their help with the software and digital design. S. Ghoreishizadeh acknowledges the support of the Imperial College Junior Research Fellowship scheme.

REFERENCES

- [1] G. De Micheli, S. S. Ghoreishizadeh, C. Boero, F. Valgimigli and S. Carrara, "An integrated platform for advanced diagnostics," European Conference on Design Automation and Test (DATE), France, 2011
- [2] M. Nazari et al., "CMOS neurotransmitter microarray: 96-channel integrated potentiostat with on-die microsensors," *IEEE Trans. Biomed. Circuits Syst.*, vol. 7, no. 3, pp. 338-348, Jun. 2013
- [3] M. Stanacevic, K. Murari, A. Rege, G. Cauwenberghs, and N. V. Thakor, "VLSI potentiostat array with oversampling gain modulation for widerange neurotransmitter sensing," *IEEE Trans. Biomed. Circuits Syst.*, vol. 1, no. 1, pp. 63-72, Mar. 2007
- [4] H. Li et al., "CMOS amperometric ADC with high sensitivity, dynamic range and power efficiency for air quality monitoring," *IEEE Trans. Biomed. Circuits Syst.*, vol. 10, no. 4, pp. 817-827, Aug. 2016
- [5] DirectNet Study Group, "Evaluation of factors affecting CGMs calibration, Diabetes Tech, and Therapeutics," vol 8, no 3, pp 318-25, 2008
- [6] H. Ikeda et al., "An auto-gain control transimpedance amplifier with low noise and wide input dynamic range for 10-Gb/s optical communication systems," *IEEE J. of Solid-State Circuits*, vol. 36, no. 9, pp. 1303-8, 2011
- [7] M. Crescentini et al., "Noise Limits of CMOS Current Interfaces for Biosensors: A Review," *IEEE TBCAS*, vol. 8, no. 2, pp. 278-92, 2014
- [8] Christian Enz and G.C. Temes, "Circuit techniques for reducing the effects of op-amp imperfections: Autozeroing, correlated double sampling, and chopper stabilization," 84:1584 - 1614, 12 1996
- [9] S. S. Ghoreishizadeh, G. Nanda, S. Carrara, and G. De Micheli, "Empirical study of noise dependence in electrochemical Sensors," *IEEE International Workshop on Advances in Sensors and Interfaces (IWASI)*, Italy, 2013
- [10] S. S. Ghoreishizadeh, I. Taurino, G. De Micheli, S. Carrara, and P. Georgiou, "A differential electrochemical readout ASIC With heterogeneous integration of bio-nano Sensors for amperometric sensing," *IEEE Trans. Biomed. Circuits Syst. (TBCAS)*, vol. 11, no. 5, pp. 1148 - 59, Oct. 2017
- [11] H. Li et al., "Ultracompact microwatt CMOS current readout with picoampere noise and kilohertz bandwidth for biosensor arrays," *IEEE TBCAS.*, vol. 12, no. 1, pp. 35-46, Feb. 2018